Acta Polytechnica **66**(1):19–29, 2026
https://doi.org/10.14311/AP.2026.66.0019

Published by the Czech Technical University in Prague

AN EFFICIENT DEEP LEARNING FRAMEWORK FOR CONTACTLESS PALMPRINT RECOGNITION: MULTIRESOLUTION PRINCIPAL COMPONENT ANALYSIS NETWORK

Hakim Doghmane[a,*], Zoheir Mentouri[b], Mohamed Cherif Amara Korba[c], Hocine Bourouba[a], Larbi Boubchir[d]

[a] *Université 8 Mai 1945 Guelma, Faculty of Science and Technology, Electronics and Telecommunications Department, PIMIS Laboratory, Guelma 24000, Algeria*

[b] *Research Center in Industrial Technologies, Cheraga, 16014 Algiers, Algeria*

[c] *University of Souk Ahras, Faculty of Sciences and Technology, Electrical Engineering Department, LEER Laboratory, 41000 Souk Ahras, Algeria*

[d] *University of Paris 8, LIASD Research Lab., 2 Rue de la Liberté, 93526 Saint-Denis Cedex, France*

[*] corresponding author: doghmane_hakimaz@yahoo.fr

Abstract. Contactless palmprint recognition is a widely used method of personal identification. Its performance relies primarily on the feature extraction stage, where intra-variability (pose, scale, and illumination) must be considered. This study presents a novel and challenging contactless palmprint representation called the Deep Statistical Image Features (DSIF), which combines the Discrete Wavelet Transform (DWT) with the Principal Component Analysis Network (PCANet). The methodology uses the following steps: First, the DWT of levels 1 and 2 is applied to extract different sub-band images. Next, the PCANet algorithm is applied to the palmprint image and the low-frequency sub-band images. Then, histograms are extracted and concatenated. Finally, the reduced representation is constructed using Whitened Principal Component Analysis (WPCA). The key contribution of this study is its feature extraction methodology, which uses multiresolution analysis instead of multi-patch decomposition in order to obtain pertinent information from various image resolutions. The proposed method uses the entire IIT-Delhi contactless database to construct the model, which is then tested on two other contactless palmprint databases, CASIA and Tongji. The method achieved rank-1 identification rates of 99.80 % on CASIA, 98.77 % on Right Tongji, and 99.07 % on Left Tongji, results that are impressive compared to current approaches and methods.

Keywords: Palmprint recognition, PCANet, multiresolution analysis, principal component analysis.

1. Introduction

Accelerated advances in information and network technologies have made information security more critical than ever before [1, 2]. Biometrics is increasingly adopted due to its stability, uniqueness, and convenience [3]. Biometric systems comprise various techniques, methods, algorithms, and devices that leverage human characteristics to automatically and accurately identify individuals. Hand-based biometric identifiers, in particular, are attracting a great deal of interest due to their ease of use and acceptance [3–5]. The most commonly used hand-based biometrics are fingerprints [6], hand shape [7], and palmprints [8–10]. In the field of biometry, palmprint recognition has emerged as a promising technology, taking advantage of the human palm's unique anatomical and physiological features. Unlike fingerprints, palmprints feature distinctive patterns formed by ridge structures, minutiae, and skin texture, which remain largely unchanged throughout an individual's life [11, 12]. This stability, combined with the relatively larger surface area of the palm, results in a range of features that can improve the accuracy and reliability of biometric systems. Both contact and non-contact (contactless) acquisition methods can be used to obtain palmprint images. When using a contact-based palmprint acquisition method, subjects must ensure their hand is positioned correctly to take pictures by touching the sensor fastened to pegs [13]. A contactless palmprint acquisition method is feasible in unrestricted settings and with commercial off-the-shelf cameras. The latter offers several benefits, including greater confidentiality and user-friendliness as well as the absence of hygiene risks, which was particularly important during the recent COVID-19 pandemic [14–18]. Over the last few decades, numerous approaches have been proposed for palmprint recognition. Current palmprint feature extraction methodologies can be classified into two main categories: handcrafted feature-based and deep learning-based approaches. The former includes several subcategories, such as line-based approaches [19, 20], coding-based approaches [21–24], statistic-based approaches [25], subspace-based approaches [26], and texture-based approaches [27]. Doghmane et al. [28] presented a novel palmprint recognition framework

called the Discriminant Gabor LPQ Spatial Pyramid Histogram (DGLSPH). This method uses a combination of Gabor wavelet analysis, Local Phase Quantization (LPQ), and Spatial Pyramid Histogram (SPH) to extract discriminative features from palmprint images. The extracted features are further processed using the Whitened Linear Discriminant Analysis (WLDA) in order to enhance discriminability while reducing dimensionality. This study evaluates the method using three palmprint databases (PolyU2D, PolyU2D/3D, and IITD), demonstrating that it is significantly more accurate than existing techniques. Bendjoudi et al. [29] proposed a new palmprint identification approach based on Patch Binarised Statistical Image Features Descriptor (PBSIFD). Their study aimed to improve palmprint recognition by addressing computational complexity and sensitivity to translation, illumination, and rotation. The authors introduced a simplified version, RPBSIFD, that uses WLDA for feature reduction. The method was evaluated on multiple palmprint databases (PolyU2D, PolyU2D/3D, IITD, and CASIA). Ignat et al. [30] presented a palmprint recognition system using SURF key points and a novel fixed-number key point selection algorithm called FIKEN. Their approach combines SURF key point extraction with a nearest-neighbour classification scheme using a ratio-based distance measure. The approach was validated experimentally on the IITD, CASIA, and GPDS contactless palmprint datasets. Amrouni et al. [13] presented a contactless palmprint recognition approach that uses binarised statistical image features (BSIF) with a multiresolution analysis. Their system uses the Discrete Wavelet Transform (DWT) for multiscale representation, followed by BSIF-based feature extraction. Cao et al. [9] proposed a palmprint recognition method that emphasises template protection through composite fixed-length ordered features. By fusing dual-orientation features extracted via a modified finite Radon transform (MFRAT) and point features derived from SURF, the system employed an index-of-max (IoM) transformation for irreversible template protection. Its evaluation on the CASIA and PolyU datasets demonstrated enhanced recognition accuracy and robust security against a variety of attacks.

In the second category, deep learning techniques, particularly convolutional neural networks (CNNs), are used to automatically learn hierarchical features from raw data, reducing the need for manual feature extraction. This improves recognition performance and enhances robustness to fluctuations in image quality and environmental conditions. The most commonly used deep-learning feature in palmprint recognition is derived from Convolutional Neural Network (CNN). It consists of a number of convolutional and sub-sampling layers, producing a fully connected layer, which in turn can be used as a robust feature classifier module. However, a weakness of this approach is that it requires a higher number of training images to train the network for the desired performance, which can be impractical for palmprint recognition systems. Moreover, CNNs require a considerable number of parameters and have high computational demands, which makes them unfeasible for real-time applications. To overcome the shortcomings of the CNN-based method, Chan et al. [31] proposed a simple deep learning method called the Principal Component Analysis Network (PCANet) that uses basic data processing components, such as cascaded PCA, binary hashing, and block-wise histogram, for image classification. The PCANet has two stages: the convolutional stage and the output stage. In the convolutional stage, the PCANet learns the filter banks by PCA and can be more easily and efficiently designed as compared to a CNN. It generates the filter using the whole view of an original image. Then, the image is convolved with the filter bank generated from the previous step. In the output stage, the output from the last convolutional layer is then converted to a binary hash, and a block-wise histogram is generated for classification. Veigas and Kumari [32] presented a touchless palmprint recognition system using an AlexNet-inspired CNN combined with a fuzzy Support Vector Machine (SVM). The CNN extracts discriminative palmprint features, which are then classified using a fuzzy SVM to ensure robust performance. Trabelsi et al. [33] introduced an efficient palmprint biometric identification system using a simplified PalmNet architecture and Gabor filters for feature extraction. Feature selection and dimensionality reduction techniques were applied to reduce the computational overhead without compromising accuracy. A Support Vector Machine (SVM) classifier was employed for the classification, achieving high recognition rates on CASIA, PolyU, IITD, and Tongji datasets. Belhocine et al. [2] introduced a contactless palmprint recognition system combining handcrafted and deep learning-based features, including the Pyramid Histogram of Oriented Gradients (PHOG), Local Phase Quantisation (LPQ), DCTNet, DSTNet, PCANet, and ICANet. A deep rule-based (DRB) classifier was employed for the classification tasks.

This paper proposes a new palmprint feature representation using the PCANet algorithm and multi-resolution analysis. Inspired by the work of Chan et al. [31], we built the PCANet model from the entire IIT-Delhi database. The generated model is then used for other contactless palmprint databases within the multi-resolution framework.

The key contributions of this paper can be summarised as follows:

- A feature extraction approach for contactless palmprint recognition is proposed, leveraging the power of Discrete Wavelet Transform (DWT) multiresolution analysis combined with the advanced PCANet method.
- A novel method is proposed to significantly improve the classification accuracy.

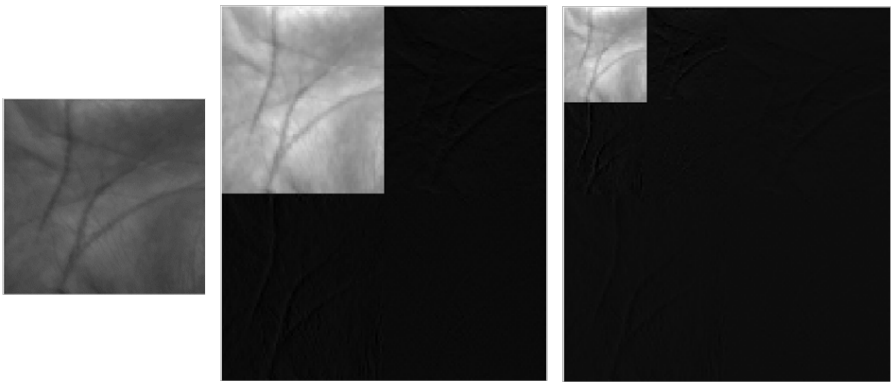

FIGURE 1. The 2D-wavelet decomposition.

- Extensive experiments and thorough analyses are conducted during the feature extraction stage, testing and considering a range of configurations to find the best-performing parameters that maximise the recognition rate.

The remaining sections of the paper are organised as follows: Section 2 explains the proposed methodology and each technique used in this work. Section 3 presents the outcomes of our experiments and a comparative analysis. Section 4 concludes the paper.

2. Proposed approach

Recently, deep learning approaches have gained popularity, particularly convolutional neural networks (CNNs), which automatically learn and extract features from palmprint images, resulting in improved accuracy and robustness. It is well-recognised that texture is one of the most important characteristics of a palmprint image. Motivated by these considerations, the main objective of this study is to use a simple deep learning network with a multi-resolution analysis to extract textural information across different levels. The PCANet method is used mostly for image classification and face recognition [31]. The proposed representation step is, therefore, developed based on the use of the PCANet method in a multiresolution analysis framework to extract deep statistical features from the input palmprint image. The following subsections outline the key steps of the proposed method and explain its underlying principle.

2.1. Discrete Wavelet Transform (DWT)

The Discrete Wavelet Transform (DWT) is a powerful signal processing technique used to analyse signals at multiple levels of resolution. It transforms a discrete-time signal into a set of coefficients representing the signal at different frequency bands and time intervals. The DWT uses a variety of mother wavelets, including Haar, Daubechies, Coiflets, and symlet. The following Equations (1)–(3) provide a mathematical expression of the theoretical background of applying the DWT to a 2D image, and they are explained as follows:

- Let $\psi(t)$ be a mother wavelet function. We can derive the wavelet function family $\psi_{(a,b)}(t)$ as:

$$\psi_{a,b}(t) = \frac{1}{\sqrt{a}}\,\psi\left(\frac{t-b}{a}\right), \tag{1}$$

  where a and b are the scale and the position parameters, respectively.

- Assume $I(x,y)$ is an image of size $M \times N$. The two-dimensional DWT is expressed as follows:

$$A_{\varphi}(j_0,m,n) = \frac{1}{\sqrt{MN}} \sum_{x=0}^{M-1}\sum_{y=0}^{N-1} I(x,y)\,\varphi_{j_0,m,n}(x,y), \tag{2}$$

$$D^{i}_{\psi}(j,m,n) = \frac{1}{\sqrt{MN}} \sum_{x=0}^{M-1}\sum_{y=0}^{N-1} I(x,y)\,\psi_{j,m,n}(x,y), \tag{3}$$

  where $A_{\varphi}(j_0,m,n)$ represents the approximation coefficients of $I(x,y)$ at a scale j_0, $D^{i}_{\psi}(j,m,n)$ represents the horizontal, vertical, and diagonal detail coefficients for a scale $j \geq j_0$, respectively, and $\varphi(.)$, $\psi(.)$ define the scaling and the wavelet functions, respectively.

Figure 1 shows several resolutions represented in an image by repeating cycles of wavelet transform (high pass filter) and scaling (low pass filter). While the wavelet gathers the image's high-frequency (detail) information, the scaling captures the image's low-frequency (approximation) information. A single 2D DWT decomposition yields four sub-bands, each one-half the size. Due to the concentration of energy in low frequencies, the lower-resolution version effectively captures most of the original image, resulting in excellent image representation efficiency.

The 2D wavelet transform separates an image into four sub-bands. The high-frequency components correspond to the horizontal, vertical, and diagonal detail coefficients, while the low-frequency component correspond to the approximation coefficients.

2.2. Principal Component Analysis Network (PCANet) structures

PCANet maintains the CNN architecture while employing an unsupervised learning methodology. In this

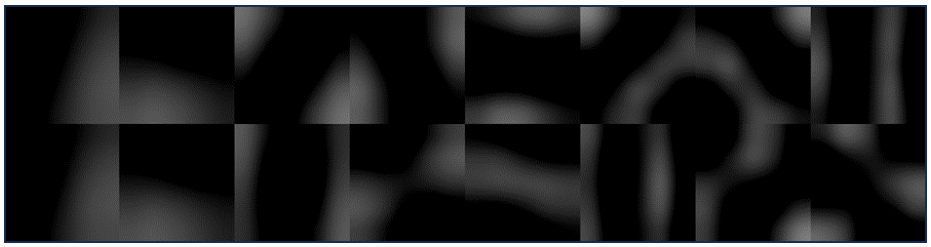

Figure 2. Example of the learned PCANet filters derived from the entire IIT-Delhi database. At the top: the eight filters of the first stage, At the bottom: The eight filters of the second stage.

approach, convolution kernels are derived from image plots through the cascaded principal component analysis (PCA) algorithm rather than through an iterative weight adjustment process. Chan et al. [31] introduced PCANet, a simple yet effective deep learning model designed for image classification tasks. The network leverages cascaded Principal Component Analysis (PCA) filters, binary hashing, and block-wise histograms for feature extraction. Despite its structural simplicity and absence of nonlinear activation functions in intermediate layers, PCANet achieved a competitive performance across multiple datasets, including face recognition and handwritten digit classification. It served as a baseline model for deep learning research, demonstrating that even basic linear operations can yield strong classification results.

The overall architecture of PCANet is divided into two phases: training and testing. In the training phase, the filter banks for the first and second layers of PCANet are constructed using the PCA algorithm. An example of the learned PCANet filters derived from the entire IIT-Delhi database is shown in Figure 2. In the testing phase, the convolution process is performed, in which both the training and testing images are convolved with the filter bank built during the training phase. Before being sent to the classifier, the output of the last convolutional layer is restructured to produce the final feature vector.

2.2.1. PCANet technique principle

Let us consider N training images $\{I_i\}_{i=1}^{N}$ and a patch size of $k_1 \times k_2$ at all stages. Only the PCA filters need to be learned from the input images I_i in the PCANet model. During the training phase, it is presumed that N input training pictures of size $m \times n$ are provided as $\{I_i\}_{i=1}^{N}$, and L_i denotes the number of filters in the i^{th} convolutional layer. In the first layer, patches are taken using the size $k_1 \times k_2$ in I_i, and they are transformed into vectors that are represented by $X_{i,j} \in R^{k_1 \times k_2}$. All centred vectors are grouped in the matrix $\bar{X}_i = [\bar{x}_{i,1}, \ldots, \bar{x}_{i,mn}] \in R^{k_1 k_2 mn}$, and let $X = \left[\bar{X}_1, \ldots, \bar{X}_N\right] \in R^{k_1 k_2 \times Nmn}$ be a concatenation of all the training images. The first layer filters are built using the covariance matrix XX^t by reshaping the L_1 principal eigenvectors, where the $\text{mat}_{k_1,k_2}(q_l(XX^t))$ maps the l^{th} principal eigenvector $q_l(XX^t) \in R^{k_1 k_2}$ to the matrix $w_l^1 \in R^{k_1 \times k_2}$. The first layer outputs are generated by a convolution of the input image with each filter $I_i^l = I_i * w_l^1$. The process for the second layer is identical to that for the first layer, where the input images are the first layer outputs and are integrated into $Y = \left[Y^1, \ldots, Y^{L_1}\right] \in R^{k_1 k_2 \times Nmn}$. The second layer filters are calculated as $W_l^2 = \text{mat}_{k_1,k_2}(q_l(YY^t)) \in R^{k_1 k_2}$, $l = 1, 2, \ldots, L_2$. Every training and testing image is convolved to the filter bank created during the training phase for the testing phase. The result of this procedure can then be written as $O_i^l = \left\{I_i^l * W_l^2\right\}_{l=1}^{L_2}$. After that, the output is binarised as $\left\{H\left(I_i^l * W_l^2\right)\right\}_{l=1}^{L_2}$, and converted to the decimal as $T_i^l = \sum_{l=1}^{L_2} 2^{l-1} H\left(I_i^l * W_l^2\right)$, where $H(.)$ is the Heaviside function. The feature vector representation $f_i = B\,\text{hist}\left(T_i^1, \ldots, T_i^{L_2}\right) \in R^{2^{L_2 L_1} B}$ is obtained by employing a block-wise histogram strategy where the number of blocks in each T_i^l is denoted as B. We set the PCANet parameters to a filter size of $k_1 = k_2 = 5$, the number of filters $L_1 = L_2 = 8$, and the number of blocks $B = 1$. An example of encoded image generation process using the PCANet algorithm is illustrated in Figure 3.

2.3. Proposed palmprint representation

The main contribution of our study is the feature extraction step, which is based on the use of PCANet method in a multiresolution analysis framework to extract Deep Statistical Image Features (DSIF) from the input palmprint image. The concept is outlined in Figure 4 and consists of the following phases: First, the PCANet method is applied directly to the original palmprint image, and its associated histogram is extracted. The original palmprint image is then subjected to the DWT decomposition, which separates it into four sub-band images: Low-Low (LL), Low-High (LH), High-Low (HL), and High-High (HH). This decomposition corresponds to the first level of the DWT. Furthermore, the obtained LL sub-band image provides access to more accurate approximations of the original image while replacing and compressing it. In the initial stage of the decomposition, the PCANet method is applied to the L1-LL sub-band (Level 1 of Low-Low), generating its corresponding histogram. Likewise, the DWT decomposition process is applied to the L1-LL sub-band to derive the L2-LL representation, which encompasses more useful and compressed information. This step is followed

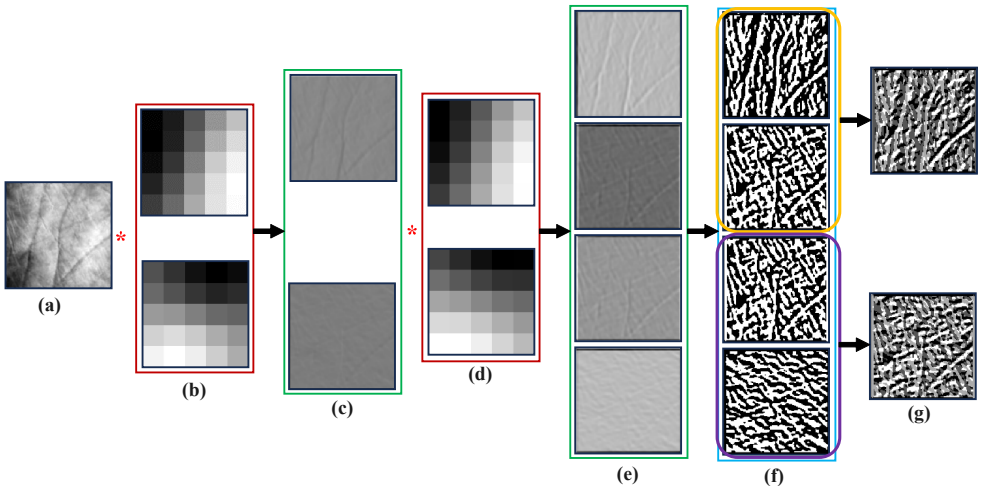

FIGURE 3. Example of encoded image generation process using PCANet algorithm. (a) Original image, (b) Filters derived from stage 1 (size 5×5), (c) Image responses after stage 1, (d) Filters derived from stage 2 (size 5×5), (e) Image responses after stage 2, (f) Binary images, (g) Encoded images.

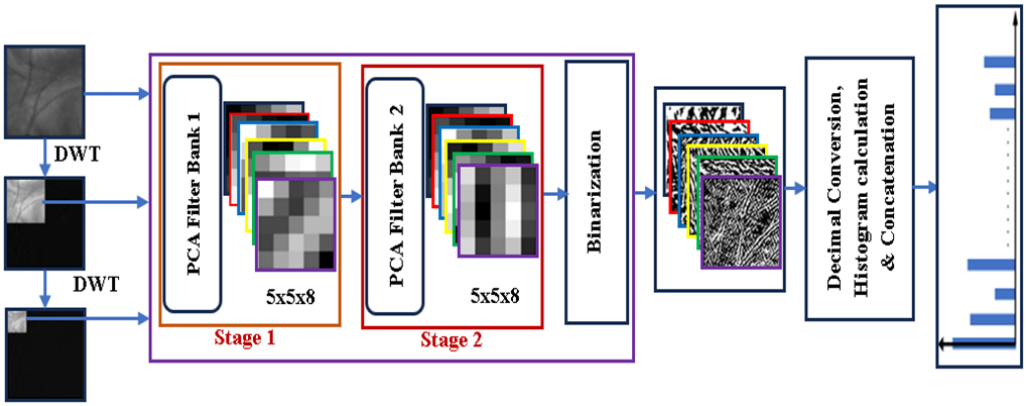

FIGURE 4. Proposed palmprint representation.

by a PCANet technique to produce the histogram of the second resolution. After that, the histograms produced from each level are concatenated to form a feature vector representation. Next, a pooling operation is performed to reduce dimensionality and extract the most important features by projecting palmprint features into a lower-dimensional space using a whitened PCA method, therefore providing the DSIF representation. Finally, the K-NN classifier is used with a cosine distance for the classification step.

3. Discussion of experiments and results

In this section, we evaluate the performance of the proposed representation in touchless palmprint recognition. We will conduct several experiments organised into three main parts. The first part involves constructing the PCANet's learned filters. The second part presents experiments to select the optimal feature extraction parameters. The last part focuses on evaluating the performance of the proposed biometric identification system. We use the entire IIT-Delhi dataset for learning the PCA filters in PCANet, and then apply this trained PCANet within the multiresolution framework to extract features of new subjects in the CASIA and Tongji touchless palmprint datasets. In all experiments, the dimensions of the proposed feature vectors are reduced to 1 000 via a whitening PCA (WPCA) [34], where the projection matrix is trained from the features of gallery samples. The NN classifier with cosine distance is used without applying any image pre-processing. In addition, we follow the evaluation protocol (with the exception of experiment #4). The CASIA dataset has been randomly split into training and testing sets in a 60:40 ratio. The recognition rates averaged over five random splits. In the Tongji database, we use the two palmprint samples (left and right palms) separately for the evaluation. The samples taken during the first session are used for training, while those from the second session are used for testing.

3.1. IIT-Delhi dataset

In the IIT Delhi touchless palmprint database, images were collected from 230 individuals using both hands (i.e. 460 distinct palms). At least five palmprint sam-

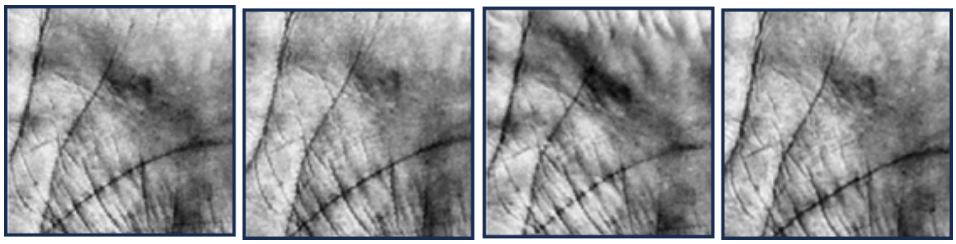

(a). First subject.

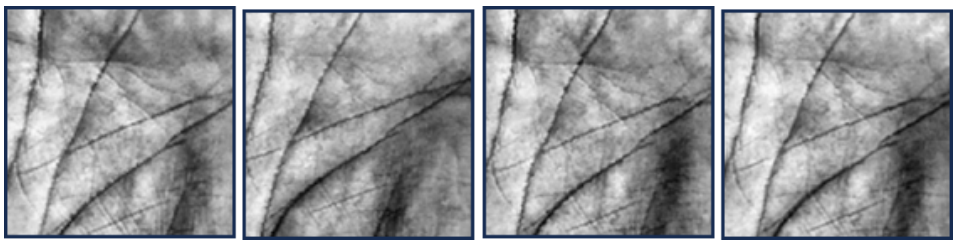

(b). Second subject.

Figure 5. Examples of palmprint images from the IITD database.

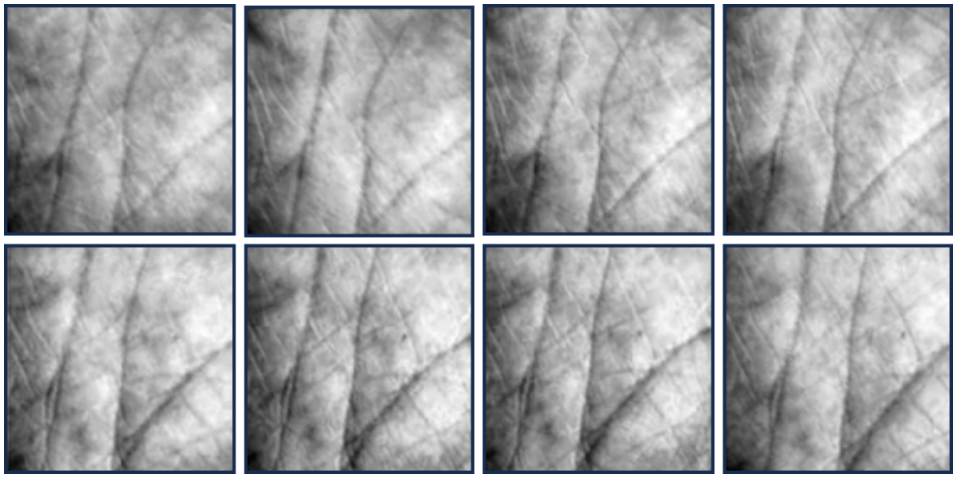

Figure 6. Examples of palmprint images from the CASIA database.

ples for each hand are available for each individual. ROI images are also available at [35], which were extracted using the algorithm described in [23]. Figure 5 gives some ROI examples of palmprint images from two different subjects. The four images in the first row were captured from the first subject while the images in the second row were captured from the second subject. We use these assembled palmprint images to train the PCANet.

3.2. CASIA dataset

The CASIA palmprint image database was established by the "China Academy of Sciences Institute of Automation (CASIA)" and contains 5 502 images from 312 subjects (i.e. 624 distinct palms). Each subject had more than eight palmprint images taken for both their left and right hands. All images in this database were obtained with a CMOS camera and without pegs. The images are 8-bit grey-level JPEG files. Figure 6 shows examples of palmprint images from the CASIA database.

3.3. Tongji dataset

The Tongji is a publicly available dataset including 12 000 images of 600 distinct palms. The dataset comprises data from a broad group of 300 participants, including 192 males and 108 females, with 235 people aged 20 to 30 and the remainder aged 30 to 50. Two independent sessions were held to collect left and right palm samples. Each volunteer contributed 10 images per palm during each session, totalling 40 images from two palms per person. The average gap between the first and the second sessions was 61 days. Figure 7 shows some ROI examples of palmprint images from two different sessions of the same subject.

3.4. Experiment #1: Learned filters of PCANet

In this subsection, we use the entire IIT-Delhi database for training the PCANet filters. The PCANet hyperparameters are chosen as shown in Table 1.

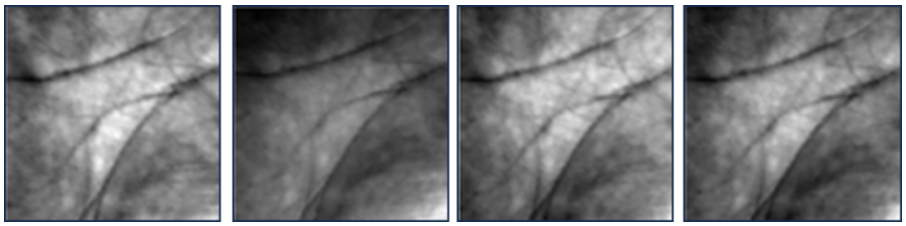

(A). Left palm images of the first subject from session 1.

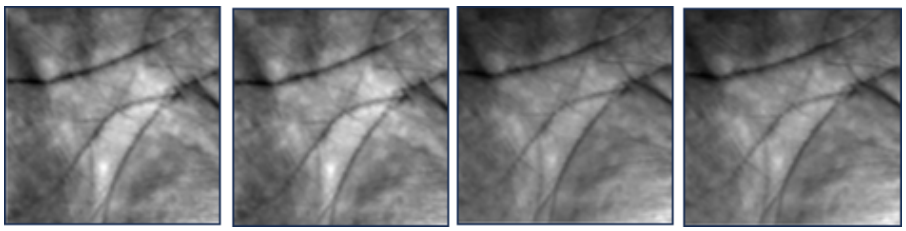

(B). Left palm images of the first subject from session 2.

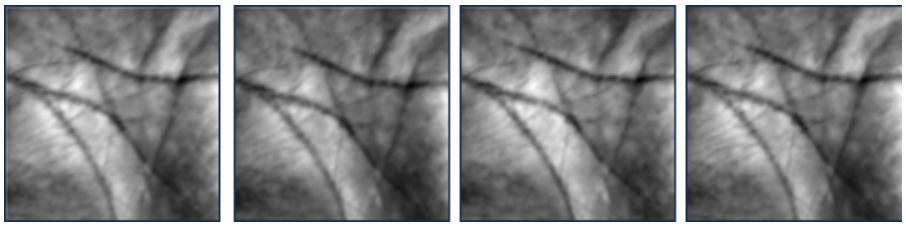

(C). Right images of the first subject from session 1.

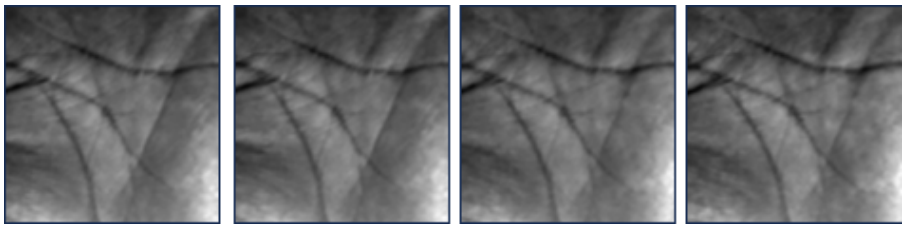

(D). Right palm images of the first subject from session 2.

FIGURE 7. Examples of palmprint images from the Tongji database.

Hyperparameters	Description	Values
S	Number of stages	$S = 2$
K_1, k_2	The filter size (with $K_1 = k_2$)	$K_1 = k_2$ varies from 3 to 11
L_1	Number of filters in first stage	$L_1 = 8$
L_2	Number of filters in first stage	$L_2 = 8$

TABLE 1. Values of the PCANet hyperparameters.

The filter learning process uses the PCA algorithm by varying the patch size $k_1 = k_2$ from 3 to 11. Figure 8 shows all of the learned PCANet filters.

3.5. Experiment #2: The impact of the wavelet family

This section examines the effect of the wavelet type used on the performance of the proposed recognition system, using the CASIA database. The filter size of the networks is $k_1 = k_2 = 5$, and the number of filters in the first and second stages is $L_1 = L_2 = 8$. The examined wavelet families include the Haar, Daubechies (db), Biorthogonal (bior), Coiflets (coif), and Symlets (sym). Table 2 clearly shows that the Haar wavelet achieved the best performance with a recognition rate of 99.77 %. This can be attributed to its ability to detect discontinuities, which is highly effective for identifying the contours of hand lines and distinctive palm features. Consequently, in the subsequent experiments, we adopt the Haar wavelet as the optimal parameter.

3.6. Experiment #3: Impact of the filter patch size

In this experiment, we examine the impact of the filter size on the robustness of the proposed approach. We

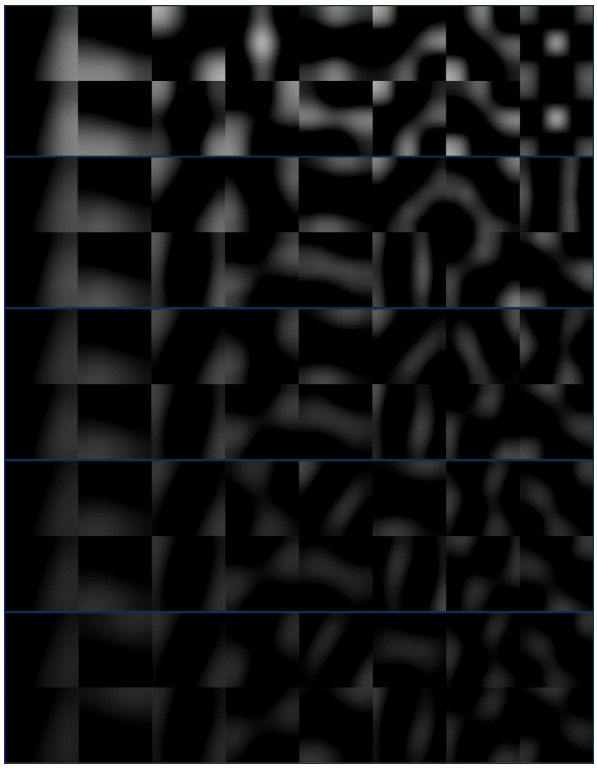

Figure 8. All filters learned from the entire IIT-Delhi database using the PCANet algorithm.

DWT families	Biorthogonal		Daubechies		Symlets		Coiflets		Haar
Results	bior1.3	99.43 ± 0.33	db1	99.58 ± 0.23	sym2	99.60 ± 0.25	coif1	99.61 ± 0.10	99.77 $\pm$0.20
	bior1.5	99.43 ± 0.20	db2	99.51 ± 0.17	sym3	99.64 ± 0.19	coif2	99.41 ± 0.37	
	bior2.2	99.50 ± 0.12	db3	99.38 ± 0.29	sym4	99.61 ± 0.11	coif3	99.18 ± 0.37	
	bior6.8	99.45 ± 0.32	db4	99.32 ± 0.33	sym5	99.55 ± 0.09	coif4	99.22 ± 0.21	

Table 2. Recognition accuracy of the proposed method for the CASIA database for different wavelet types.

vary the filter size in both stages, setting $k_1 = k_2$ to odd values from 3 to 11, and we set $L_1 = L_2 = 8$.

Tables 3 and 4 demonstrate how the filter size affects the recognition system. It can be seen that the lowest recognition rates, 90.22 % (CASIA), 80.03 % (Right Tongji), and 81.07 % (Left Tongji) are achieved when employing a small filter size ($k_1 = k_2 = 3$). Conversely, the highest recognition rates, 99.80 % (CASIA), 98.77 % (Right Tongji), and 99.07 % (Left Tongji), are achieved with the filter size of 7×7. This evaluation reveals that making a well-informed choice can effectively harness the extraction of high-frequency components by leveraging a greater number of filters ($L_1 = L_2 = 8$), while simultaneously ensuring the preservation of relevant low-frequency information due to the large size of the filters ($k_1 = k_2 = 7$). This strategic approach promises to deliver superior results.

3.7. Experiment #4: Impact of the number of palmprint training samples

We report the recognition accuracy of the proposed approach as a function of the number of generic con-

$K_1 \times k_2$	Accuracy [%]
3×3	90.22 ± 0.01
5×5	99.77 ± 0.20
7×7	$\mathbf{99.80 \pm 0.02}$
9×9	99.62 ± 0.01
11×11	99.60 ± 0.15

Table 3. Identification rates with different filter sizes for the CASIA database.

$K_1 \times k_2$	Accuracy [%]	
	Left	Right
3×3	81.07	80.03
5×5	97.93	97.30
7×7	**99.07**	**98.77**
9×9	99.02	98.73
11×11	98.87	98.20

Table 4. Identification rates with different filter sizes for the right and left Tongji databases.

Training set	Accuracy [%]
40 %	97.81 ± 0.54
50 %	99.30 ± 0.17
60 %	99.80 ± 0.09
70 %	99.84 ± 0.08

TABLE 5. Impact of the number of palmprint training samples for CASIA database.

Training set	Left	Right
40 %	97.17 ± 0.67	97.37 ± 0.21
50 %	97.61 ± 0.62	97.81 ± 0.47
60 %	98.30 ± 0.29	98.43 ± 0.40
70 %	98.67 ± 0.14	98.55 ± 0.25
100 %	99.07	98.77

TABLE 6. Impact of the number of palmprint training samples for Tongji database.

	CASIA	Tongji right	Tongji left
PHOG-based feature extraction [2]	-	99.07 % (level = 4)	98.93 % (level = 5)
LPQ-based feature extraction [2]	-	99.41 (window size = 15×15)	99.44 (window size = 35×35)
BSIF + DWT [13]	98.10	-	-
Reduced BSIF Descriptor [29]	99.34	-	-
Alexnet + Fuzzy SVM [32]	98.93	-	-
VGG-16 [36]	92.14	-	-
VGG-19 [36]	92.16	-	-
Alexnet [37]	96.73	-	-
PCANetStandard	96.47	87.63	87.40
Our approach (DSIF)	**99.80**	98.77 %	99.07 %

TABLE 7. Comparative results showing the recognition rates of the proposed schemes and recently proposed methods for CASIA and Tongji databases.

tactless palmprint training images. For the CASIA database, we randomly split the images into training and testing sets by adjusting the training ratio from 40 % to 70 %, with the remainder constituting the test set. Similarly, for the Tongji database, we randomly selected a training set by varying the training ratio from 40 % to 100 % of the Right (or Left) Tongji set from the first session and the entire Right (or Left) Tongji set from the second session was used as a testing set. Our findings indicate that the accuracy of the proposed method is slightly sensitive to the number of generic palmprint training images. However, the performance of the proposed method shows a promising trend, gradually improving as the number of generic palmprint training samples increases, as shown in Tables 5 and 6.

3.8. Experiment #5: Comparison with the state of the art

To ensure a more comprehensive analysis, we conducted a thorough comparison of our innovative approach with several state-of-the-art methods for contactless palmprint recognition. Table 7 presents the average rank-1 recognition rates of our proposed method compared to other advanced feature extraction techniques. The results conclusively confirm that our approach not only is highly competitive, but also significantly outperforms existing methods. Notably, when compared with the standard PCANet method, our approach achieves a significantly higher accuracy, boasting improvements of 3.33 %, 11.67 %, and 11.14 % for the CASIA, Left Tongji, and Right Tongji databases, respectively. Which is not a mere incremental progress, but a leap forward in the effectiveness of palmprint recognition.

4. Conclusion

In this paper, the proposed novel approach for contactless palmprint representation combines the unsupervised convolutional deep learning network PCANet and a multi-resolution image analysis. The method is based on three key steps:

(1.) the Discrete Wavelet Transform (DWT) used to perform a multi-resolution analysis by decomposing the palmprint texture into various frequency subbands;

(2.) the PCANet algorithm used to efficiently learn complex discriminative filters without relying on labelled training data;

(3.) the whitened PCA method used to reduce the dimensionality of the global histogram and preserve only the most informative components.

The comprehensive experimental results demonstrate that this proposed DSIF representation achieves a high identification accuracy across multiple heterogeneous and contactless palmprint image acquisition systems, confirming its enhanced robustness against variations in the capture distance, angle, and illumination. Ultimately, the developed model could benefit from several potential improvements in future work. For example, exploring new concatenation strategies by varying filter banks and scale factors, employing multi-size filters instead of fixed-dimension patches, or using different activation functions, such as sigmoid, tanh, or even ReLU, instead of the basic binarisation operation are all viable options. These approaches could enhance the effectiveness of the proposed method.

References

[1] A. I. Awad, A. Babu, E. Barka, K. Shuaib. AI-powered biometrics for Internet of Things security: A review and future vision. *Journal of Information Security and Applications* **82**:103748, 2024. https://doi.org/10.1016/j.jisa.2024.103748

[2] Y. Belhocine, A. Meraoumia, K. Abderrazak, M. Saigaa. Efficient contactless palmprint recognition system based on deep rule-based classification. *Acta Informatica Pragensia* **13**(2):193–212, 2024. https://doi.org/10.18267/j.aip.236

[3] X. Guo, P. Zhang, C. Wang, et al. A novel deep learning model for palmprint/palmvein recognition. *IEEE Access* **9**:122847–122854, 2021. https://doi.org/10.1109/ACCESS.2021.3110206

[4] A. Attia, S. Mazaa, Z. Akhtar, Y. Chahir. Deep learning-driven palmprint and finger knuckle pattern-based multimodal person recognition system. *Multimedia Tools and Applications* **81**(8):10961–10980, 2022. https://doi.org/10.1007/s11042-022-12384-3

[5] C. Kant, S. Chaudhary. A multimodal biometric system based on finger knuckle print, fingerprint, and palmprint traits. In M. K. Sharma, V. S. Dhaka, T. Perumal, et al. (eds.), *Innovations in Computational Intelligence and Computer Vision*, vol. 1189, pp. 182–192. Springer Singapore, Singapore, 2021. https://doi.org/10.1007/978-981-15-6067-5_21

[6] F. Liu, Y. Zhao, G. Liu, L. Shen. Fingerprint pore matching using deep features. *Pattern Recognition* **102**:107208, 2020. https://doi.org/10.1016/j.patcog.2020.107208

[7] N. Charfi, H. Trichili, A. M. Alimi, B. Solaiman. Bimodal biometric system for hand shape and palmprint recognition based on SIFT sparse representation. *Multimedia Tools and Applications* **76**(20):20457–20482, 2017. https://doi.org/10.1007/s11042-016-3987-9

[8] Z. Yang, L. Leng, A. B. J. Teoh, et al. Cross-database attack of different coding-based palmprint templates. *Knowledge-Based Systems* **264**:110310, 2023. https://doi.org/10.1016/j.knosys.2023.110310

[9] Z. Cao, W. Zhao, H. Zhao, L. Pang. Composite fixed-length ordered features with index-of-max transformation for high-performing and secure palmprint template protection. *Journal of Information and Intelligence* **3**(1):51–67, 2025. https://doi.org/10.1016/j.jiixd.2024.09.002

[10] L. Wu, Y. Xu, Z. Cui, et al. Triple-type feature extraction for palmprint recognition. *Sensors* **21**(14):4896, 2021. https://doi.org/10.3390/s21144896

[11] L. Fei, Y. Xu, B. Zhang, et al. Low-rank representation integrated with principal line distance for contactless palmprint recognition. *Neurocomputing* **218**:264–275, 2016. https://doi.org/10.1016/j.neucom.2016.08.048

[12] L. Zhang, L. Li, A. Yang, et al. Towards contactless palmprint recognition: A novel device, a new benchmark, and a collaborative representation based identification approach. *Pattern Recognition* **69**:199–212, 2017. https://doi.org/10.1016/j.patcog.2017.04.016

[13] N. Amrouni, A. Benzaoui, R. Bouaouina, et al. Contactless palmprint recognition using binarized statistical image features-based multiresolution analysis. *Sensors* **22**(24):9814, 2022. https://doi.org/10.3390/s22249814

[14] W. Jia, B. Zhang, J. Lu, et al. Palmprint recognition based on complete direction representation. *IEEE Transactions on Image Processing* **26**(9):4483–4498, 2017. https://doi.org/10.1109/TIP.2017.2705424

[15] Y.-T. Luo, L.-Y. Zhao, B. Zhang, et al. Local line directional pattern for palmprint recognition. *Pattern Recognition* **50**:26–44, 2016. https://doi.org/10.1016/j.patcog.2015.08.025

[16] S. Zhao, B. Zhang. Learning complete and discriminative direction pattern for robust palmprint recognition. *IEEE Transactions on Image Processing* **30**:1001–1014, 2021. https://doi.org/10.1109/TIP.2020.3039895

[17] S. A. Maadeed, X. Jiang, I. Rida, A. Bouridane. Palmprint identification using sparse and dense hybrid representation. *Multimedia Tools and Applications* **78**(5):5665–5679, 2019. https://doi.org/10.1007/s11042-018-5655-8

[18] I. Rida, S. A. Maadeed, X. Jiang, et al. An ensemble learning method based on random subspace sampling for palmprint identification. In *2018 IEEE International Conference on Acoustics, Speech and Signal Processing (ICASSP)*, pp. 2047–2051. 2018. https://doi.org/10.1109/ICASSP.2018.8462051

[19] D.-S. Huang, W. Jia, D. Zhang. Palmprint verification based on principal lines. *Pattern Recognition* **41**(4):1316–1328, 2008. https://doi.org/10.1016/j.patcog.2007.08.016

[20] X. Wu, D. Zhang, K. Wang. Palm line extraction and matching for personal authentication. *IEEE Transactions on Systems, Man, and Cybernetics – Part A: Systems and Humans* **36**(5):978–987, 2006. https://doi.org/10.1109/TSMCA.2006.871797

[21] A. W.-K. Kong, D. Zhang. Competitive coding scheme for palmprint verification. In *Proceedings of the 17th International Conference on Pattern Recognition, 2004. ICPR 2004*, vol. 1, pp. 520–523. IEEE, Cambridge, UK, 2004. https://doi.org/10.1109/ICPR.2004.1334184

[22] Z. Guo, D. Zhang, L. Zhang, W. Zuo. Palmprint verification using binary orientation co-occurrence vector. *Pattern Recognition Letters* **30**(13):1219–1227, 2009. https://doi.org/10.1016/j.patrec.2009.05.010

[23] L. Fei, Y. Xu, W. Tang, D. Zhang. Double-orientation code and nonlinear matching scheme for palmprint recognition. *Pattern Recognition* **49**:89–101, 2016. https://doi.org/10.1016/j.patcog.2015.08.001

[24] W. Jia, D.-S. Huang, D. Zhang. Palmprint verification based on robust line orientation code. *Pattern Recognition* **41**(5):1504–1513, 2008. https://doi.org/10.1016/j.patcog.2007.10.011

[25] Q. Dai, N. Bi, D. Huang, et al. M-band wavelets application to palmprint recognition based on texture features. In *2004 International Conference on Image Processing, 2004*, vol. 2, pp. 893–896. IEEE, Singapore, 2004. https://doi.org/10.1109/ICIP.2004.1419443

[26] G. Lu, D. Zhang, K. Wang. Palmprint recognition using eigenpalms features. *Pattern Recognition Letters* **24**(9–10):1463–1467, 2003. https://doi.org/10.1016/S0167-8655(02)00386-0

[27] L. Fei, G. Lu, W. Jia, et al. Feature extraction methods for palmprint recognition: A survey and evaluation. *IEEE Transactions on Systems, Man, and Cybernetics: Systems* **49**(2):346–363, 2019. https://doi.org/10.1109/TSMC.2018.2795609

[28] H. Doghmane, H. Bourouba, K. Messaoudi, A. Bouridane. Palmprint recognition based on discriminant multiscale representation. *Journal of Electronic Imaging* **27**(5):053032, 2018. https://doi.org/10.1117/1.JEI.27.5.053032

[29] S. Bendjoudi, H. Bourouba, H. Doghmane, et al. Palmprint identification performance improvement via patch-based binarized statistical image features. *Journal of Electronic Imaging* **28**(5):053009, 2019. https://doi.org/10.1117/1.JEI.28.5.053009

[30] A. Ignat, I. Păvăloi. Keypoint selection algorithm for palmprint recognition with SURF. *Procedia Computer Science* **192**:270–280, 2021. https://doi.org/10.1016/j.procs.2021.08.028

[31] T.-H. Chan, K. Jia, S. Gao, et al. PCANet: A simple deep learning baseline for image classification? *IEEE Transactions on Image Processing* **24**(12):5017–5032, 2015. https://doi.org/10.1109/TIP.2015.2475625

[32] J. Prakash Veigas, S. Kumari M. Deep learning approach for touchless palmprint recognition based on Alexnet and fuzzy support vector machine. *International Journal of Electrical and Computer Engineering Systems* **13**(7):551–559, 2022. https://doi.org/10.32985/ijeces.13.7.7

[33] S. Trabelsi, D. Samai, F. Dornaika, et al. Efficient palmprint biometric identification systems using deep learning and feature selection methods. *Neural Computing and Applications* **34**(14):12119–12141, 2022. https://doi.org/10.1007/s00521-022-07098-4

[34] K. Kavukcuoglu, P. Sermanet, Y.-l. Boureau, et al. Learning convolutional feature hierarchies for visual recognition. In J. Lafferty, C. Williams, J. Shawe-Taylor, et al. (eds.), *Advances in Neural Information Processing Systems*, vol. 23, pp. 1–9. 2010.

[35] D. Hu, G. Feng, Z. Zhou. Two-dimensional locality preserving projections (2DLPP) with its application to palmprint recognition. *Pattern Recognition* **40**(1):339–342, 2007. https://doi.org/10.1016/j.patcog.2006.06.022

[36] A. S. Tarawneh, D. Chetverikov, A. B. Hassanat. Pilot comparative study of different deep features for palmprint identification in low-quality images, 2018. https://doi.org/10.48550/arxiv.1804.04602

[37] W. Gong, X. Zhang, B. Deng, X. Xu. Palmprint recognition based on convolutional neural network – Alexnet. In *Annals of Computer Science and Information Systems*, pp. 313–316. 2019. https://doi.org/10.15439/2019F248